

Frontal bone virtual reconstruction and geometric morphometric analysis of the mid-Pleistocene hominin KNM-OG 45500 (Olorgesailie, Kenya)

Tommaso Mori^{1,2}, Antonio Profico^{3,4}, Hugo Reyes-Centeno^{5,6,7} & Katerina Harvati^{1,5}

1) Paleoanthropology, Department of Geosciences, Senckenberg Centre for Human Evolution and Palaeoenvironment, University of Tübingen, Tübingen 72070, Germany

e-mail: tommaso.mori@ifu.uni-tuebingen.de

2) Anthropology laboratory, Department of Biology, University of Florence, Via del Proconsolo 12, Florence, Italy

3) Dipartimento di Biologia Ambientale, Sapienza Università di Roma, Rome, Italy

4) PalaeoHub, Department of Archaeology, University of York, York, United Kingdom

5) DFG Center for Advanced Studies "Words, Bones, Genes, Tools", University of Tübingen, Rümelinstrasse 23, D-72070 Tübingen, Germany

6) Department of Anthropology, University of Kentucky, 211 Lafferty Hall, Lexington, KY 40506 USA

7) William S. Webb Museum of Anthropology, University of Kentucky, 1020 Export St, Lexington, KY 40504, KY USA

Summary - KNM-OG 45500 is a hominin fossil composed of parts of a frontal bone, left temporal bone, and cranial vault pieces. Since its discovery along the Olorgesailie Formation (Kenya) in 2003, it has been associated with the *Homo erectus* hypodigm. The specimen, derived from a geological context dated to ca. 900 Ka BP, has been described as a very small individual of probable female sex. However, despite its status as an important hominin specimen, it has not been used in a quantitative comparative framework because of its fragmentary condition. Here, we undertake a virtual reconstruction of the better-preserved fragment, the frontal bone. We additionally apply geometric morphometric analyses, using a geographically diverse fossil and modern human sample, in order to investigate the morphological affinities of KNM-OG 45500. Our results show that the frontal shape of KNM-OG 45500 exhibits similarities with Early Pleistocene fossils from Eurasia and Africa that are assigned to *H. erectus sensu lato* (s.l.). Its size, on the other hand, is notably smaller than most other *Homo erectus* fossils and modern humans and similar to the specimens from Dmanisi (Georgia) and to *Homo naledi*. Taken together, our analyses of the frontal bone suggest a taxonomic attribution of KNM-OG 45500 to *H. erectus* s.l. and extend even further the range of size variability associated with this taxon around 900 Ka BP.

Keywords - *Homo erectus*, Shape analysis, Frontal bone, Geometric morphometrics, Virtual anthropology.

Introduction

The taxonomic attribution of Pleistocene (following Gibbard *et al.*, 2010) fossils to *Homo erectus* has been highly debated by paleoanthropologists in the last decades. No full consensus exists among scientists regarding the definition of the *erectus* hypodigm (Stringer, 1984; Wood, 1984; Rightmire, 1990; Tattersall, 1992; Wolpoff

et al., 1994; Schwartz & Tattersall, 2000; Wood & Richmond, 2000; Antón, 2003; Schwartz, 2004; Antón, 2007; Terhune *et al.*, 2007; Baab, 2008b, 2016; Lordkipanidze *et al.*, 2013; Antón *et al.*, 2014; Bauer & Harvati, 2015; Mori & Harvati, 2019). The most restricted conception of *H. erectus* (*sensu stricto*) limits the species to specimens from the Asian fossil record, which include the holotype from Trinil, while African

specimens are often attributed to *H. ergaster* (Dubois, 1894; Stringer, 1984; Wood, 1991; Wolpoff *et al.*, 1994; Schwartz & Tattersall, 2000). On the other hand, a commonly accepted definition of *H. erectus* (*sensu lato*) puts together specimens from Africa and Eurasia, unifying Pleistocene fossils otherwise attributed to different *Homo* taxa, including *ergaster*, *georgicus*, and *soloensis* (Antón, 2003; Rightmire *et al.*, 2006; Zeitoun *et al.*, 2010; Lordkipanidze *et al.*, 2013; Rightmire, 2013; Baab, 2015).

Different authors have tried to investigate the patterns of variation between geographic or chronological groups within the broadly defined *H. erectus* hypodigm (Rightmire, 1981, 1990; Stringer, 1984; Wood, 1992; Kidder & Durband, 2004; Terhune *et al.*, 2007; Baab, 2008b, 2016; Zeitoun *et al.*, 2010). Some of the recent studies have interpreted the fossil record as reflecting a single lineage (e.g. Suwa *et al.*, 2007; Lordkipanidze *et al.*, 2013) while others propose a view of species diversity in the Early Pleistocene (e.g. Baab, 2008a; Leakey *et al.*, 2012; Antón, Potts & Aiello, 2014; Spoor *et al.*, 2015). A recent reconstruction and analysis of Olduvai Hominin 7 (OH 7) from Olduvai Gorge (Tanzania), the holotype specimen of *H. habilis* (Spoor *et al.*, 2015), seemingly confirmed the latter hypothesis. However, whereas Spoor and colleagues (2015) highlighted from this reconstruction that early *Homo* groups were distinct also on the basis of different brain sizes, Antón *et al.* (2014) had rejected size as a defining feature of “early *Homo*” groups. Spoor *et al.* (2015) also suggested that, given the dissimilarities between both *H. habilis* and other “early *Homo*” specimens, these early Pleistocene eastern African fossils comprised multiple species. This is particularly important in light of recently described *Homo species novo* in the Middle and Late Pleistocene, including *H. naledi* (Berger *et al.*, 2015), *H. luzonensis* (Détroit *et al.*, 2019), and *H. floresiensis* (Brown *et al.*, 2004). Similarly, taxonomic diversity in later fossils dated between 1.8 MA BP and 900Ka BP from Africa and Eurasia is highly debated (Wood, 1994; Schwartz & Tattersall, 2000; Vekua *et al.*, 2002; Antón, 2003; Potts *et al.*,

2004; Schwartz, 2004; Gilbert & Asfaw, 2008; Baab, 2016). While the fragmentary fossil record remains a limitation, what has become clear is that the pattern of within-sample variation in Pleistocene hominin groups is often complex and understanding whether this variability represents multiple taxa or not is hotly debated. The small specimens from Dmanisi (Georgia), for example, have shown the existence of high morphological variability in what is considered by most scholars a single paleodeme (Howell, 1999; Vekua *et al.*, 2002; Rightmire *et al.*, 2006; Lordkipanidze *et al.*, 2013). Given the fragmentary status of other fossils, however, some specimens are rarely studied or included as comparative material, thus reducing the possibility to have a more complete picture regarding the evolutionary relationship between different geographic and temporal fossil groups. This is the case for KNM-OG 45500, a hominin fossil recovered from the Olororgesailie formation, Kenya (Potts *et al.*, 2004).

The KNM-OG 45500 (also referred to as KNM-OL 45500 in the literature) fossil was recovered *in situ* in 2003 in a stratigraphic layer rich with Acheulean handaxes (Potts *et al.* 2004). Volcanic layers underlying and overlying KNM-OG 45500 have been dated using the single-crystal $^{40}\text{Ar}/^{39}\text{Ar}$ method to between ca. 974 and 747 ka. Because of its close association to the lower layer, a geological age between 970 and 900 ka has been proposed for this specimen (Potts *et al.*, 2004). KNM-OG 45500 has been described as one of the smallest African *Homo erectus s.l.*, alongside the recently published DAN5/P1 fossil from the Dana Anoule North site of the Busidima Formation (Gona, Ethiopia) (Semaw *et al.* 2020) and the KNM-ER 42700 specimen from the Koobi Fora Formation (Spoor *et al.*, 2007; Neubauer *et al.*, 2018; Mori & Harvati, 2019), dated to ca. 1.6–1.5 Ma. KNM-OG 45500’s frontal bone shows midline keeling, a shelf-like morphology of the post-toral sulcus, a lack of torsion in the toral anterior surface, and double-arched supraorbital shape (Potts *et al.*, 2004). Its endocranial volume (ECV) is estimated to be less than 800 cm³, similar in size to the DAN5/P1 fossil (Semaw *et al.* 2020), as well as to the D2282

and D2280 specimens from Dmanisi (Georgia), which date to ca. 1.8 Ma and are assigned by most authors to *Homo erectus s.l.* (Vekua *et al.*, 2002; Antón, 2004; Potts *et al.*, 2004; Rightmire *et al.*, 2006, 2019; Lordkipanidze *et al.*, 2013). KNM-OG 45500 exhibits an overall smaller size than Early Pleistocene fossils from Kenya (e.g. KNM-ER3733 and KNM-WT15000, dated to between 1.8-1.5 Ma), but closer to the later OH12 fossil from Olduvai (dated to ca. 1.2-1.1 Ma) (Rightmire, 1979; Tamrat *et al.*, 1995)1995. In contrast, the morphology of the double-arched supraorbital torus is considered similar in shape to other African fossils, such as the Early Pleistocene specimen Daka BOU-VP-2/66 (Ethiopia) and KNM-ER3733 (Kenya)(Potts *et al.*, 2004).

The frontal bone, especially the morphology of the supraorbital torus, has been used to distinguish between different morphs of *H. erectus s.l.* (Stringer, 1984; Wood, 1984; Rightmire, 1990; Antón, 2003; Schwartz, 2004; Baab, 2015, 2016). More generally, the frontal bone is considered useful in reconstructing hominin phylogeny and population history in modern humans (Weidenreich, 1940; Smith, 2009; von Cramon-Taubadel, 2009; Athreya, 2012; Freidline *et al.*, 2012; von Cramon-Taubadel & Smith, 2012). Many of the morphological characters that are used to define *H. erectus s.l.* involve cranial superstructures: localized hypertrophies of the bones in the form of tori, crests, and keels. These features, however, are not always easy to quantify. The grade of frontal keeling, supraorbital morphology, and frontal profile are difficult to capture with standard morphometric approaches (Weidenreich, 1940; Athreya, 2012). Geometric morphometric (GM) methods, on the other hand, can help quantify such morphologies and provide the possibility to quantitatively compare different fossils in order to better evaluate the morphological differences and similarities between them (Rohlf & Slice, 1990; Bookstein, 1991; Slice, 2007; Mitteroecker & Gunz, 2009; Freidline *et al.*, 2012; Aytek & Harvati, 2016). In this framework, we aim to analyze the morphology of the more complete frontal fragment belonging to KNM-OG 45500.

Our primary objectives are (1) to undertake a reconstruction of the frontal bone of KNM-OG 45500 and (2) to apply GM methods for the comparative analysis of this reconstruction, in order to assess the morphological affinities of this specimen with other African, Asian, and European early and mid-Pleistocene hominin fossils. Furthermore, we aim to address the question of intra-specific morphological variation in the Pleistocene human fossil record by comparing the range of variation in form (shape and size) within *H. erectus s.l.* to that observed within a broad geographic sample of modern humans.

Materials and methods

Frontal bone reconstruction

The frontal bone reconstruction of KNM-OG 45500 aims to account for possible taphonomic deformation and fragmentation. While the KNM-OG 45500 frontal bone presents an almost complete supraorbital torus, the left margin of the supraorbital region is broken and the left part of the frontal squama is missing two fragments posteriorly. The right part of the supraorbital torus is abraded due to taphonomic processes, but laterally it is more complete than the left side and it reaches close to the frontozygomatic suture. Posteriorly, the coronal suture seems to be preserved only in the lateral part of the right side, with a preserved sphenofrontalis suture and stephanion. While bregma is missing, Potts *et al.* (2004) suggested that the squama is broken roughly 10 mm anterior to it.

The reconstruction was performed via mirroring of the preserved left structures on the right side and *vice versa*, a commonly applied procedure in virtual reconstruction (Gunz *et al.*, 2009; Bauer & Harvati, 2015; Weber, 2015; Harvati *et al.*, 2019), using the Avizo software (version 9.1, Thermo Fischer Scientific) and the transform function in the Meshlab software (v2016.12) (Cignoni *et al.*, 2008). The specimen was mirrored using the transform flip axis function in the Meshlab software (v2016.12) (Cignoni *et al.*, 2008). We manually aligned,

Tab. 1 - Modern humans' populations origin.

| POPULATION | N (M/F/U) | COLLECTIONS |
|--------------------------|-----------|--|
| Australia (Aborigines) | 6 (3/3/0) | American Museum of Natural History, New York |
| Europe (Italy) | 5 (2/3/0) | Museo di Storia Naturale, Florence |
| Chile (Tierra del Fuego) | 2 (0/2/0) | Naturhistorisches Museum, Vienna |
| Sri Lanka | 4 (0/0/4) | University Museum, Tübingen |
| China | 5 (0/0/5) | Musee de l'Homme, Paris |
| Philippines | 5 (0/0/5) | Musee de l'Homme, Paris |
| Tanzania (Masai) | 2 (0/0/2) | University Museum, Tübingen |

in Avizo software (version 9.1, Thermo Fischer Scientific) the mirrored version to the original one using both homologous anatomical structures and the midsagittal plane as reference. The midsagittal plane is defined by a landmark approximating bregma (the midline point on the posterior edge), glabella, and the mid-toral sulcus. The mirrored specimen aligned well with the original specimen along the orbital roof, the supraorbital region, and the medial portion of the frontal squama. We used the mirrored version of KNM-OG 45500 to reconstruct the missing portions of the left lateral frontal squama and lateral supraorbital region and the abraded right supraorbital torus.

Reference sample

Our comparative sample comprises 30 recent modern human adults. The sampling strategy was designed to capture as much variation as possible in recent human populations via worldwide coverage, the inclusion of both sexes, and groups known for their relatively smaller body size. The samples are derived from museum collections and are no older than a few hundred years (see Table 1 for specific geographic origin,

sex, and housing institution information). One population, from the Philippines, comprises individuals of short stature (Reyes-Centeno *et al.*, 2014). 3D surface models of the specimens were obtained from medical computed tomography (CT) scans or micro-CT scans using the Avizo software (Noback & Harvati, 2014, 2015; Bosman *et al.*, 2019; Bosman, Reyes-Centeno & Harvati, 2020).

The fossil comparative sample comprises 20 specimens from different chronological periods and geographical areas. The 3D surface models were derived from CT scans of the original specimens or optical surface scans of high-quality casts (Tab. 2). Our sample comprises several *H. erectus s.l.* fossils spanning the Pleistocene, other Middle to Late Pleistocene *Homo* specimens sometimes attributed to *H. rhodesiensis/heidbergensis* (Broken Hill, Bodo, Petralona, Dali) and early *H. sapiens* (Jebel Irhoud 1, Skhül V), as well as two other small-sized hominins: the Early Pleistocene MH 1 *A. sediba* type specimen and the composite cranial reconstruction of *H. naledi* based on the DH1 holotype & DH3 paratype specimens named “naledi” in all following analyses and text (Berger *et al.*, 2015; Schroeder *et al.*, 2017). While the mix of optical and tomographic scans from both original fossils and fossil casts could represent a source of measurement error, previous work has shown that maximum surface deviations between original fossils and high-quality hominin fossil casts are minimal (Ponce De Leon & Zollikofer, 1999). Moreover, concerns over possible technical and data source errors were mitigated in our study by the relatively dense landmark coverage and the sliding procedure of the surface semi-landmarks. We note that two of the fossil comparative specimens (M.H. 1 and D 2700) are sub-adults. In M.H. 1, third molars have not erupted but second molars are in occlusion, whereas D2700 exhibits an erupted M3 that is not in occlusion (Vekua *et al.*, 2002; Berger *et al.*, 2010). Furthermore, D2282 is described as a near-adult due to the lower M3 being “newly” erupted in terms of dental wear (Rightmire *et al.*, 2006).

Tab. 2 - Fossil sample used. Abbreviations: MH= Malapa Hominin, D= Dmanisi, KNM= Kenya National Museums, ER=East Rudolf, OG= Olorgesailie, DH= Dinaledi Hominin, AMNH=American Museum of Natural History

| FOSSIL SPECIMEN | CAST/ ORIGINAL | INSTITUTION | CHRONOLOGICAL AGE |
|---|-------------------|--------------------------------------|---|
| <i>Au. sediba</i> | | | |
| MH 1 ¹ | C | AMNH | 1.97 Ma (Pickering <i>et al.</i> , 2011) |
| <i>H. erectus s.l.</i> | | | |
| D 2280 | C | AMNH | 1.77 Ma (Garcia <i>et al.</i> , 2010) |
| D 2700 ¹ | C | AMNH | 1.77 Ma (Garcia <i>et al.</i> 2010) |
| D 3444 | C | AMNH | 1.77 Ma (Garcia <i>et al.</i> 2010) |
| D 2282 ¹ | C | AMNH | 1.77 Ma (Garcia <i>et al.</i> 2010) |
| Daka BOU-VP-2/66 | O | National Museum of Ethiopia | 1 Ma – 780 Ka (Asfaw <i>et al.</i> , 2002) |
| KNM-ER 3733 | O | Kenya National Museum | 1.63 Ma (Lepre & Kent, 2015) |
| KNM-ER 3883 | O | Kenya National Museum | 1.53 Ma (McDougall <i>et al.</i> , 2012) |
| Ngandong 14 | C | AMNH | 118-108 Ka (Rizal <i>et al.</i> , 2020) |
| Sangiran 17 | C | AMNH | 1.2 Ma/900 Ka (Larick <i>et al.</i> , 2001; Matsu'ura <i>et al.</i> , 2020) |
| Sambungmacan 3 | C | AMNH | 60-70 Ka (Yokoyama <i>et al.</i> , 2008) |
| Zhoukoudian I | C | AMNH | 700-400 ka (Shen <i>et al.</i> , 2009) |
| Zhoukoudian 12 | C | AMNH | 700-400 ka (Shen <i>et al.</i> 2009b) |
| Middle-Pleistocene <i>Homo</i> (MPH) | | | |
| Bodo | O | National Museum of Ethiopia | 640-550 Ka (Rightmire, 1996) |
| Broken Hill 1 (Kabwe) | C | AMNH | 700 - 200 ka (Buck & Stringer, 2015) |
| Petralona | O | Aristotle University of Thessaloniki | 700-150 Ka (Grün, 1996) |
| Dali | C | AMNH | 270-180 Ka (Xiao, Jin & Zhu, 2002) |
| <i>H. naledi</i> | | | |
| <i>H. naledi</i> (DH1 & DH3 composite reconstruction) | C | University of the Witwatersrand | 200-300 Ka (Dirks <i>et al.</i> , 2017) |
| Early <i>H. sapiens</i> (EHS) | | | |
| Jebel Irhoud 1 | C | AMNH | 300-90Ka (Grün & Stringer, 1991; Richter <i>et al.</i> , 2017) |
| Skhūl V | O | Peabody Museum, Harvard University | 120-80 Ka (Grün, 2006) |
| Unknown | | | |
| KNM-OG 45500 ² | O | National Museums of Kenya | 900 Ka (Potts <i>et al.</i> , 2004) |

¹ Sub-adult specimens

² Also published as KNM-OL 45500. KNM-OG 45500 follows the accession number at the National Museums of Kenya.

Tab. 3 - Landmark number and definition.

| DEFINITION (BAAB, 2016) | |
|------------------------------|--|
| 1. Bregma | Posterior border of the frontal bone along the midsagittal plane. |
| 2. Midline post-toral sulcus | Minima of concavity on midline post-toral frontal squama. |
| 3. Glabella | Anterior-most point on frontal bone in Frankfort horizontal in the midsagittal plane. |
| 4/6 Mid-torus inferior R/L | Inferior margin of superior margin of orbit roughly at the middle of the orbital margin. |
| 5/7 Mid-orbital superior R/L | Superior point on the supraorbital torus at the middle of the orbital margin. |
| 8/9 Frontotemporale R/L | Point where the temporal line reaches its most anteromedial position on the frontal. |
| 10/11 Stephanion R/L | Point where the temporal line reaches the coronal suture. |

Landmark and semilandmark configurations

We collected a total of 80 landmarks on the frontal bone. Of these, 11 correspond to common osteometric points (i.e. Type 1-3 landmarks *sensu* Weber & Bookstein, 2011). A list and definition of these are presented in Table 3. Two semi-landmark curves (i.e. Type 4 landmarks, *sensu* Weber & Bookstein, 2011) along each superior temporal muscle line were digitized from *stephanion* to the frontozygomatic suture. A total of 14 evenly-spaced semilandmarks were placed on each curve. In order to fully investigate the shape of the frontal squama and the supraorbital torus, we used a patch of 41 surface semilandmarks defined on KNM-OG 45500 (i.e. Type 6 landmarks, *sensu* Weber & Bookstein, 2011) encompassing the space between the identified landmarks (i.e. between the superior temporal muscle line and the supraorbital region).

In KNM-OG 45500, bregma is the only missing landmark. The estimation was performed by using anatomical landmarks and the semilandmark configurations mentioned above (Gunz *et al.*, 2009). The template (digitized on KNM-OG 45500) without bregma was projected onto the specimens (for a total of 10 landmarks, 28 curves semilandmarks and 41 surface semilandmarks). Projection of the template semilandmarks was performed using the place-Patch function from the R package “Morpho” (Schlager, 2017). This projection procedure deforms the template onto every specimen target

by thin-plate-spline (TPS) interpolation based on the target’s landmarks and curve semilandmarks (Bookstein, 1989; Slice, 2007). After this step, the deformed coordinates are projected onto the target mesh. After projection, we slid the surface semilandmarks using the minimum bending energy criterion to guarantee landmark correspondence across specimens (Gunz *et al.*, 2005). Then, we reintroduced bregma taken on the complete specimens and estimated the position of bregma on KNM-OG 45500. To estimate bregma in KNM-OG 45500, we used the Thin Plate Spline (TPS) algorithm (Bookstein, 1989) choosing as reference fossil the specimens with close shape affinity. Specifically, we performed four different estimations of bregma by calculating the weighted mean using, respectively: i) the two closest specimens to KNM-OG 45500 in Procrustes distance, followed by ii) the four closest specimens, iii) the six closest, and iv) the eight closest specimens. In addition to the four estimated landmark configurations, we included a parsimonious fifth landmark configuration without reference specimens, instead defining the position of bregma as the most posterior point on the KNM-OG 45500 frontal squama along the midsagittal plane, as in the mirroring reconstruction procedure. TPS substitution was used because it performs better in estimation when the same taxon reference or closely related taxon reference samples are available (Neeser *et al.*, 2009).

The Euclidean distance between the reconstructed and unreconstructed bregma is 8 mm in 3 reconstructions and 12 mm in one reconstruction. Finally, we included all the five landmark configurations of KNM-OG 45500 as individual specimens in the subsequent statistical analyses.

The complete landmark configuration for subsequent analyses was obtained by projecting surface semilandmarks from a template onto each specimen using the same method described above. The template used was KNM-OG 45500's configuration with bregma defined as the midline point at the posterior edge of the frontal squama. The choice of the template does not influence the final results in the analyses (Mitteroecker & Gunz, 2009) because ultimately we guarantee correspondence among landmarks thanks to the sliding procedure (Gunz *et al.*, 2005). The position of all landmarks is presented in Figure 1. All landmarks were digitized by the same observer (T.M.). To estimate the measurement error of fixed landmark acquisition, we digitized the same specimen 10 times in 10 different days for the 11 Type 1-3 landmark configurations. Subsequently, intra-observer error was evaluated for each landmark based on a relative standard deviation threshold of 5%. For all 11 landmarks, the error was between 2-3.5% relative standard deviations and thus all landmarks were used for subsequent analysis.

Shape and form analysis

To explore variation in frontal bone shape in our sample, we conducted two analyses: one that used both our fossil and modern human groups and a subsequent one that used only the fossil specimens. In each case, curve semilandmarks and the projected surface semilandmarks were slid using the minimum bending energy criterion in order to guarantee landmark correspondence across specimens (Gunz *et al.*, 2005). Thereafter, the landmark configurations of the comparative sample were superimposed with generalized Procrustes analysis (GPA) (Gower, 1975; Rohlf & Slice, 1990; Bookstein, 1991), in which the sum of squared distances between corresponding

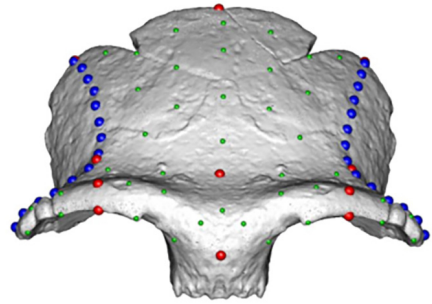


Fig. 1 - Landmark (red dots) and semilandmark (curves= blue, surface= green) configuration shown on the reconstructed *Ologresailie hominin* KNM-OG 45500. [Image adapted from scan courtesy of the National Museums of Kenya]. The colour version of this figure is available at the JASs website.

landmarks is minimized by rotation, translation, and scaling. After GPA superimposition, a principal component analysis (PCA) on the covariance matrix of the Procrustes coordinates was used to visualize and explore the shape space. The KNM-OG 45500 configurations (four with bregma estimated via TPS and one without bregma estimation) were then projected in the shape space. The landmark configurations of the five reconstructions were superimposed via GPA on the Procrustes mean shape of the reference sample. In this way, neither the PCA axes nor the Procrustes coordinates of our reference sample were influenced by KNM-OG 45500 itself, therefore treating it as an unknown. PCA does not use *a priori* group categorization. Group variation along major PC axes of variation was visualized *a posteriori* by applying convex hulls (Mitteroecker & Bookstein, 2011). Shape variation along PCA was visualized as a deformation of a 3D surface mesh derived from the mean GPA landmark configuration. Vertices of the 3D surface mesh are the landmarks and semilandmarks used in the analysis. The mean surface was transformed via TPS interpolation (Bookstein, 1989) along 2 standard deviations (std. dev.) of a given PC axis.

Following GPA, two variables useful for assessing form variation and specimen affinities

are generated: centroid size and Procrustes distance. Centroid size, calculated as the square root of the summed squared distances of the landmark coordinates from their centroid, is an indicator of relative size differences between individuals in a sample (Rohlf & Slice, 1990; Bookstein, 1991; Slice, 2007; Mitteroecker & Gunz, 2009). In this study, the size of the frontal bone is expressed by the logarithm of centroid size (logCS). Size variability (range of logCS) in modern humans was used as a proxy to compare size variability in our fossil sample.

Procrustes distance, calculated as the square root of the sum of squared differences between two superimposed landmark configurations, is a measure of overall shape similarity between two landmark configurations, and therefore between two specimens. Following our second analysis, the pairwise Procrustes distance matrix between all fossil specimens in our sample was used to perform a cluster analysis with the unweighted pair group method using arithmetic averages (UPGMA) (Sokal, 1958). This approach iteratively quantifies the similarity between two fossils and generates clusters of all sampled specimens in a rooted dendrogram, where all tips are of equal distance to the root. In this analysis, the four reconstructed specimens were reduced to a single individual by calculating the mean pairwise Procrustes distances of their configurations to other specimens.

Finally, following the second analysis with the fossil subset, we applied a Spearman correlation test between each PC and logCS to evaluate whether the PCs had an allometric component. We performed this test twice, the first time using all the fossil comparative sample without KNM-OG 45500 and then using only the fossil sample grouped as *H. erectus s.l.*, removing KNM-OG 45500 from the analysis. All of the procedures described above were conducted in R (R Core Team, 2018) using the “Morpho,” “Arothron,” and “Phangorn” packages (Schliep, 2010; Schlager, 2017; Profico *et al.*, 2018). The raw dataset and R code used can be provided by the corresponding author upon request.

Results

The KNM-OG 45500 reconstruction is presented in Figure 2. The reconstructed parts, shown in grey, are the right supraciliary arch and left margin of the supraorbital torus at the height of the zygomatic process of the frontal bone. This part of the bone, however, is abraded and not restored in its thickness, which could be slightly reduced compared to its likely original condition. The abraded part extends for ca 1,2 cm laterally. The abrasion removed very little of the bone material in this area, as shown in Figure 2. The left side of the frontal squama was also restored based on the right morphology, which appears undistorted. The overlap of the frontal squama between the original and mirrored specimens (mixed gray and red color in Fig. 2) suggests a symmetric, undistorted medial portion of the frontal bone. The original lateral left portion, instead, is taphonomically fractured and probably placed in a lower position compared to its original morphology. Laterally the left side of the frontal squama has therefore been reconstructed using the posterolateral coronal margin of the right side (Fig. 2).

A plot of the first two principal components, accounting for over 80% of the total variance, resulting from the first PCA performed on the entire comparative sample is shown in Figure 3. It shows a clear separation between the recent modern humans and the fossil specimens, mostly along PC1. PC2, on the other hand, differentiates the Middle Pleistocene *Homo* specimens (Bodo, Dali, Petralona, and Broken Hill/Kabwe) from the *Homo erectus* and *Homo sapiens* samples. Fossils in this plot show a degree of temporal clustering along PC1 and PC2. Early Pleistocene *H. erectus s.l.* specimens tend to have lower PC1 scores than Middle and late Pleistocene fossils. D2280 and KNM-ER 3733 exhibit the lowest PC1 among *H. erectus s.l.* and Samburgmacan 3 the highest score. The DH1 & DH3 composite reconstruction of the *H. naledi* specimen plots outside the variation of other fossils, with low PC1 and PC2 scores. Shape variation associated with positive PC1 scores is

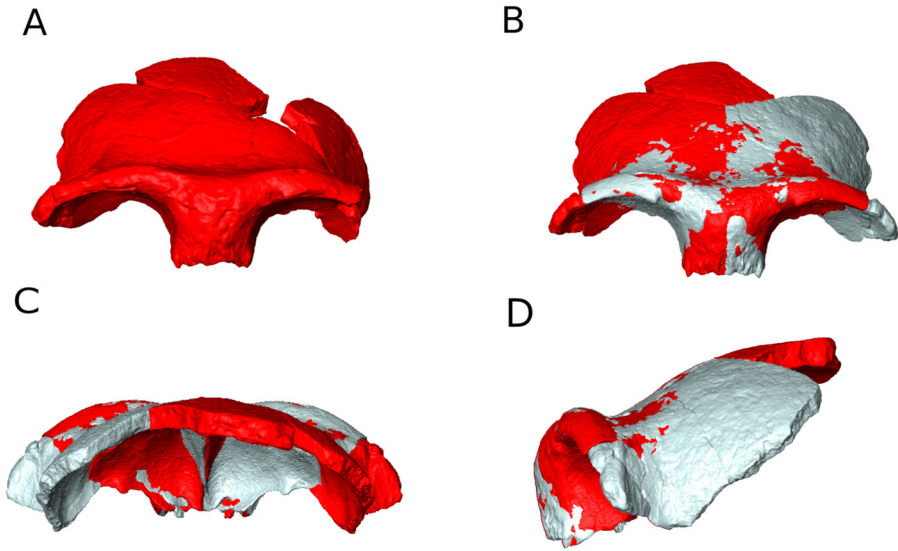


Fig. 2 - KNM-OG 45500 Reconstruction: (A) Original specimen (dark red); (B) frontal view of superimposition of the mirrored specimen (light grey) on the original one in order to reconstruct the missing areas; (C) posterior view; (D) lateral view. [Image scan courtesy of the National Museums of Kenya]. The colour version of this figure is available at the JASs website.

linked to a more globular frontal squama with a much higher bregma position. At negative PC1 scores, the frontal morphology exhibits a “shelf-like” condition, with a projected glabellar region and a clear supraorbital torus with an evident post-toral sulcus. In addition, temporal lines are more medially displaced and relatively longer along negative PC1 scores than in positive PC1 values, while positive PC1 exhibits a more latero-inferiorly placed and more arched temporal line. The lateral supraorbital region shows a flexion inferior to the frontozygomatic area for positive PC1. PC2 scores are linked to the supraorbital morphology and the relative size of the frontal squama. Positive scores of PC2 are related to a more robust, thicker, and laterally wider supraorbital torus with a relatively bigger supraorbital region compared to the shorter frontal squama. Negative values of PC2 show a more posteriorly elongated temporal line and relatively elongated frontal squama compared to the supraorbital region. The five reconstructions of KNM-OG 45500 plot in different positions of shape space,

though all fall within or closest to the *H. erectus s.l.* convex hull. Overall, they all fall with the Early Pleistocene *H. erectus s.l.* fossils. The configuration where bregma was taken on the posterior margin of the frontal squama (labeled “KNM-OG 45500” in Fig. 3) plots well within the *H. erectus s.l.* convex hull of the group; while those where bregma was reconstructed (labeled “KNM-OG 45500 rec” in Fig. 3) plot on the margin of the *H. erectus s.l.* convex hull, associated with lower PC2 scores.

The second analysis was performed only on the fossil samples. Results are presented in the PCA plot in Figure 4 and closely mirror those of the first analysis. Here, PC1 and PC2 account for ca. 64% of the total variance. Similar to the first analysis, D2280 and KNM-ER 3733 exhibit the lowest PC1 scores in the *H. erectus s.l.* group, while Sambungmacan 3 has the highest PC score. Shape variations associated with this component are similar to PC1 shape variation from the first analysis, albeit exhibiting a notably lower degree of frontal bone globularization in the absence of

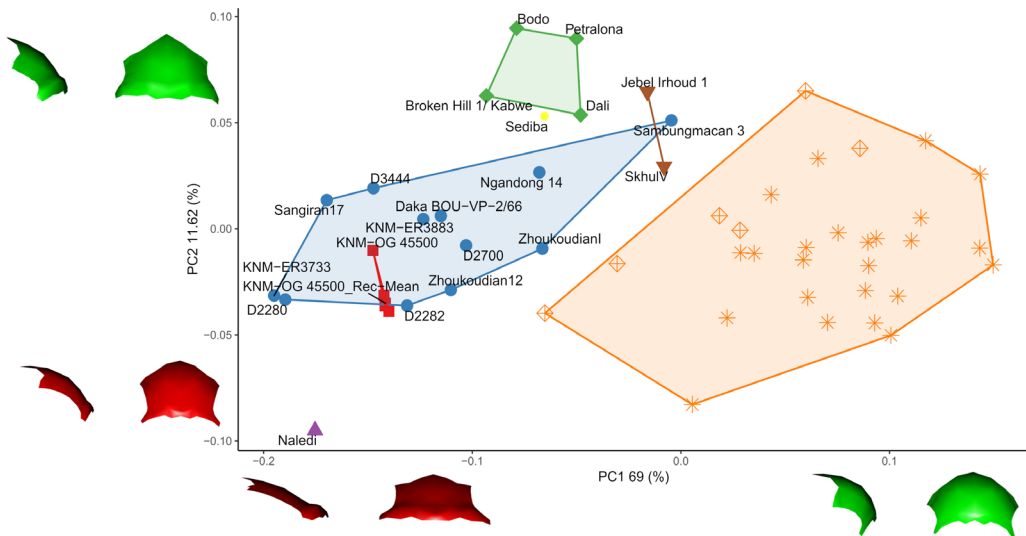


Fig. 3 - PCA plot of fossil specimens and recent modern humans. Convex hulls based on group attribution from Table 2. Colors and shape: orange symbols = recent modern humans (Australian in crossed diamond); blue circle = *H. erectus s.l.*; green diamond = Middle-Pleistocene *Homo*; brown downward triangle = early *H. sapiens*; yellow small circle = *Au. sediba*; purple triangle = *H. naledi*; red square = KNM-OG 45500. Surfaces (frontal and lateral view) are shape transformations along ± 2 std. dev. from mean along PC axes. The colour version of this figure is available at the JASs website.

the modern human sample. Along PC2, Middle Pleistocene *Homo* fossils tend to have higher values while early *Homo sapiens* and later Asian *H. erectus s.l.* have lower PC2 scores. *H. erectus s.l.* show both high and low values, with Early Pleistocene specimens toward the positive end and Middle-Late Pleistocene fossils toward the negative end. Positive scores of PC2 are associated with a thicker morphology of the supraorbital torus, an overall more robust structure, and a proportionally smaller frontal squama. Again, KNM-OG 45500 with the unreconstructed bregma plots well within the *H. erectus s.l.* convex hull and the reconstructed specimens fall on the border of the convex hull. This second analysis highlights more the degree of temporal differentiation seen in the first PCA between our sampled *H. erectus s.l.* specimens. Similarly to the first analysis, Middle to Late Pleistocene East and Southeast Asian specimens tend to have higher PC1 and lower PC2 scores, closer to fossil *H. sapiens*. By contrast, Early Pleistocene African

and Eurasian fossils have lower PC1 and higher PC2 scores distributions.

Results of pairwise Procrustes distances between all the specimens included in the second analysis are presented in the Supplemental online Material. The individuals closest in overall shape to KNM-OG 45500 are D3444, KNM-ER 3733, Zhoukoudian12, and KNM-ER 3883, respectively, all *H. erectus s.l.* The individuals closest in overall shape to the mean configuration of the reconstructed bregma specimens (KNM-OG 45500 rec) are Zhoukoudian12, D2282, the naledi composite reconstruction (DNH1 and DNH3), and KNM-ER 3733. The phenogram generated from the UPGMA cluster analysis, presented in Figure 5, shows two main clusters. One cluster includes the more recent, Middle-Late Pleistocene fossils, and the other includes the older specimens, with the exception of the *Au. sediba* and *H. naledi* specimens. KNM-OG 45500 clusters closest to the African KNM-ER 3733 and the *H. naledi* specimens.

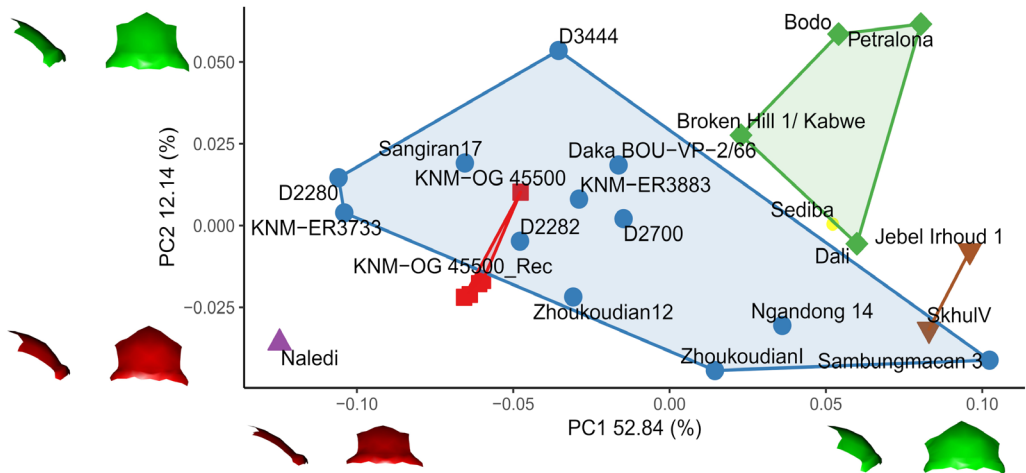


Fig. 4 - PCA plot of fossil specimens. Convex hull based on group attribution from Table 2. Colors and shape: blue circle = *H. erectus s.l.*; green diamond = Middle-Pleistocene Homo; brown downward triangle = early *H. sapiens*; yellow small circle = *Au. sediba*; purple triangle = *H. naledi*; red square = KNM-OG 45500. Frontal bone (in lateral and frontal views) shape variation corresponds to ± 2 std. dev. from mean PC values along each axis. The colour version of this figure is available at the JASs website.

LogCS distribution in our sample is presented in Figure 6. KNM-OG 45500 shows smaller size values compared to the *H. erectus s.l.* distribution and is broadly similar to the Dmanisi specimens. It is also evident that *H. erectus s.l.* specimens display a much higher degree of size variability compared to our sample of modern humans. The Daka fossil, geographically proximate and pencontemporaneous to KNM-OG 45500, has a much higher logCS than KNM-OG 45500. There is a moderate, positive association between logCS and PC1 when the full fossil sample is considered, which is statistically significant (Spearman's $\rho = 0.58$, $r^2 = 0.34$, $p\text{-value} = 0.007$), indicating that approximately 34% of the shape variation associated with the first component is explained by logCS. However, when considering only the *H. erectus s.l.* group, the association between logCS and PC1 is weaker and not statistically significant (Spearman's $\rho = 0.29$, $r^2 = 0.084$, $p\text{-value} = 0.35$). PC2 does not correlate to logCS in either of the two analyses.

Discussion

Our reconstruction of the KNM-OG 45500 frontal bone has allowed for a comprehensive, quantitative analysis of its form (size and shape) in comparison to other fossil specimens and diverse modern humans. In both of our shape analyses, the KNM-OG 45500 reconstruction with bregma taken on the posterior margin of the frontal squama plots squarely within the *H. erectus s.l.* convex hull and shows the lowest Procrustes distances to members of this taxon – irrespective of similarities or differences in overall size. In this regard, our results agree with previous interpretations by Potts *et al.* (2004), who highlighted its particularly small size and morphological affinities to *H. erectus s.l.* However, all the estimations of bregma in our other four KNM-OG 45500 reconstructions indicated that originally bregma was probably more posterior than the posterior-most sagittal point on the frontal squama taken on the original specimen. Our reconstruction

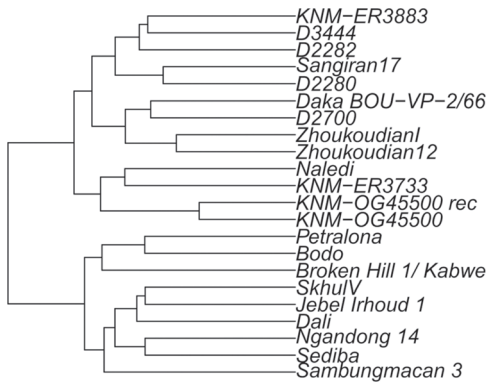


Fig. 5 - UPGMA cluster analysis based on pairwise Procrustes distances between individuals. The colour version of this figure is available at the JASs website.

results are thus in agreement with Potts and colleagues (Potts *et al.*, 2004) confirming that the original squama was probably about 8mm longer. This elongated squama, as well as its relatively thin supraorbital torus, place these reconstructions near the margin of the *H. erectus s.l.* convex hull and closer to the early specimens from Dmanisi and Kenya. Given the results of multiple estimations of bregma and the result of the unreconstructed bregma, we are confident that the original shape of KNM-OG 45500 most likely would fall inside the convex hull of all KNM-OG 45500 estimations used in the analyses.

Our reconstructions and the application of geometric morphometric comparative approaches add to previous observations in two important ways. First, we found that the first two shape components (PCs) were not strongly associated with frontal bone size (logCS) within *H. erectus s.l.*, suggesting that variation of the supraorbital morphology and frontal squama is not entirely size-dependent. Second, our rigorous data sampling approach allowed us to identify affinities in both size and shape that have not been previously described. We discuss these results below and their implications for understanding the evolution of Pleistocene *Homo*, particularly with regard to taxonomic diversity and temporal variation.

Size and allometry

While our results show that the frontal bone shape of Pleistocene *Homo* has a modest, significant allometric component, it is not significant within the sampled *H. erectus s.l.* group. The KNM-OG 45500 shape follows the expected allometric trend along PC1 (low score) when considering the full sample. If KNM-OG 45500 is accepted as a member of *H. erectus s.l.*, we must then also accept greater size variability during this time period (ca. 900 Ka BP) in the taxon than hitherto understood. In fact, within the *H. erectus s.l.* sample only the much older specimens from Dmanisi show a logCS similar to KNM-OG 45500. In this regard, KNM-OG 45500's small size, together with its geological age, is contrary to the general trend of an increase in cranial/brain size over time often described for human evolution and for the evolution of *Homo erectus* specifically (Rightmire, 2004, 2013; Antón, 2007; Lieberman, 2011; Plavcan, 2012; Lordkipanidze *et al.*, 2013;)

KNM-OG 45500's endocranial volume (ECV) has been estimated to between 622 cm³ and <800 cm³ (Potts *et al.*, 2004; Baab, 2016). We consider the lower range to be more plausible given our logCS result for KNM-OG 45500, which is similar to the Dmanisi specimens, where the ECV spans from 601 cm³ (D2700) to 730 cm³ (D2280) (Rightmire *et al.*, 2019). The pene-contemporaneous Daka BOU-VP-2/66 (Ethiopia) and Buia UA 31 (Eritrea) specimens, by comparison, have ECV values of 986 cm³ (Gilbert & Asfaw, 2008) and 995 cm³ (Bruner *et al.*, 2016), respectively — more than 1/3 larger than the expected cranial capacity of KNM-OG 45500. The difference in frontal bone size between Daka BOU-VP-2/66 and KNM-OG 45500 (Fig. 6) is larger than the size range observed among the modern humans or Middle Pleistocene *Homo* sampled in our study. It is worth noting that our modern human sample comprises small-sized individuals from the Philippines (Reyes-Centeno *et al.*, 2014). Although relatively small, our modern human sample thus allows us to place the size difference between KNM-OG 45500 and Daka

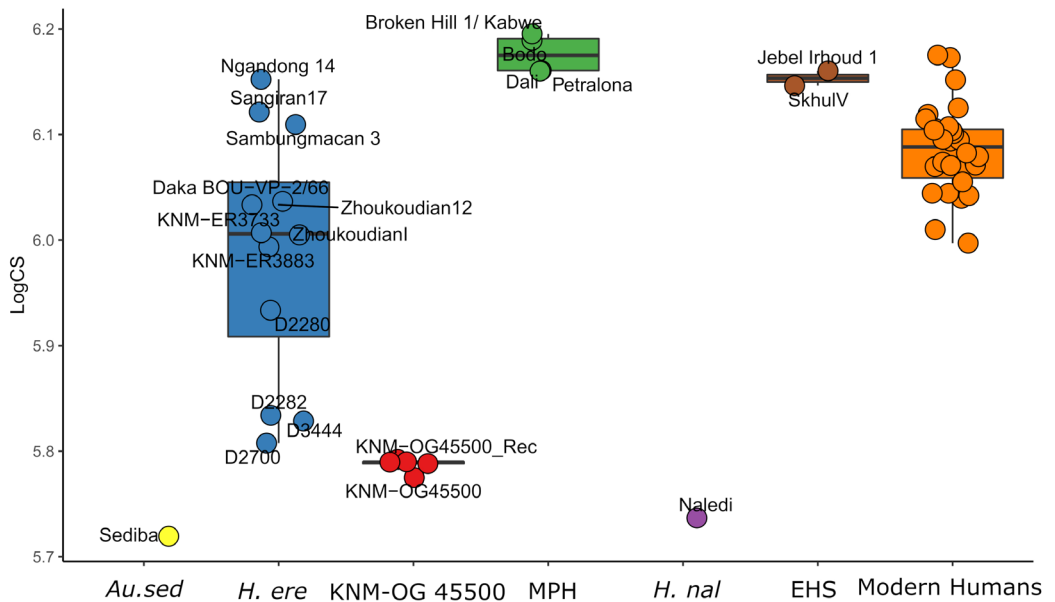


Fig. 6 - Boxplot with the distribution of LogCS values from each specimen. Groups based on Table 2 definitions. The colour version of this figure is available at the JASs website.

BOU-VP-2/66 in the context of size variation among modern humans. While in other cases the differences between KNM-OG 45500 and other fossils can be related to large chronologic and geographic ranges, the comparison with Daka can be assumed to be less influenced by those factors. Size variation is affected by many factors: resource abundance, geographical differences, ecological response, sexual dimorphism, and others. It is, however, difficult to correctly identify one factor or the synergy of different ones in the paleontological context (Plavcan, 2012). Here, we consider three aspects that can be related to KNM-OG 45500's size: ontogenetic stage, sexual dimorphism and taxonomic diversity.

Ontogenetic variation and sexual dimorphism

It might be hypothesized that KNM-OG 45500 could represent a sub-adult individual and, as such, its small size could be a result of its immature ontogenetic stage (Potts et al., 2004).

In our analyses, high PC1 scores are associated with a “modern human” shape. Ontogenetic GM studies of cranial and endocranial shape variation show that juveniles of extant *Homininae* tend to plot closer to modern humans compared to adult individuals of the same taxon along the first principal component of a PCA (Gunz et al., 2010; Neubauer et al., 2010; Terhune et al., 2013; Scott et al., 2014; Mori & Harvati, 2019). Such a tendency can be reasonably associated also to fossil hominins. Our results inform this hypothesis to the extent that they likely reflect the ontogenetic status of other fossil specimens, at least to some degree. For example, in the PCA analyses, the D 2700 sub-adult specimen plots toward higher PC 1 values in comparison to the other Dmanisi fossils, which are of an adult or near-adult ontogeny. Similarly, the MH1 *Au. sediba* subadult, which is younger in dental development than D 2700 (Berger et al., 2010; Rightmire et al., 2019), also plots toward higher PC 1 values, where frontal bone shape

is characterized by a less anteriorly projected supraorbital morphology and a rounder frontal squama. In contrast, KNM-OG 45500 plots far from modern humans along PC 1 and is closer to the adult Georgian specimens than to the D 2700 subadult. Given the limited nature of our sample and the small number of adult and subadult individuals from the same paleodeme (*i.e.* the sediba specimen is the only representative of its taxon), this result alone does not fully reject the hypothesis of a subadult stage for KNM-OG 45500. Qualitatively, however, the development of superstructures, such as the supraorbital torus, suggest an adult or near-adult ontogeny for KNM-OG 45500 (Potts *et al.*, 2004). The only suture preserved is the sphenotemporal suture on the temporal bone, which is closed but not completely obliterated. While this evidence alone is not sufficient to estimate the age of death, comparison to modern human suture closure patterns suggests that KNM-OG 45500 was either at a late stage of adolescence or already in adulthood (Meindl & Lovejoy, 1985).

Another factor that could account for the small size of KNM-OG 45500 can be related to sexual dimorphism. It has recently been proposed that *H. erectus* from Africa around 1.5 Ma BP was more dimorphic than modern humans but less so than other highly dimorphic great apes (Villmoare *et al.*, 2019). Assuming common taxonomic attribution, it is reasonable to consider that KNM-OG 45500's small size relative to the larger dimensions of the pene-contemporaneous and geographically contiguous Daka and Buia fossils supports high sexual dimorphism in this taxon. This is consistent with the interpretations for the *H. erectus* crania at Dmanisi, Georgia (Rightmire *et al.*, 2019), the footprint evidence from Ileret, Kenya (Villmoare *et al.*, 2019), and the interpretation of the fossil crania from Gona, Ethiopia (Semaw *et al.* 2020). However, skull 5 from Dmanisi and OH 12 also suggest the possible existence of different sexual dimorphism patterns. Both specimens are small but robust, thus commonly considered to be male (Antón, 2004; Rightmire *et al.*, 2019). Because KNM-OG 45500 does not reflect robust superstructures,

but only a small cranial size, we might hypothesize that KNM-OG 45500 was probably a small-bodied gracile individual, probably of female sex (Potts *et al.*, 2004). Given KNM-OG 45500's geological age our results seem to confirm high sexual dimorphism in *H. erectus s.l.* until ca. 900 Ka BP. It has been proposed that sexual dimorphism would have been reduced in our lineage, passing from more dimorphic to less dimorphic taxa associated with a relative increase in female size (Arsuaga *et al.*, 1997; Plavcan, 2012; Grabowski *et al.*, 2015), such a high level of size dimorphism around 900 Ka BP implies that this reduction in sexual size dimorphism happened in less than a million year. Nevertheless, the relationship between sexual dimorphism and frontal bone robusticity, shape, and size in *H. erectus s.l.* is currently not well understood and should be further investigated. Moreover, it is possible that other factors could influence the small size of KNM-OG 45500, including a combination of subadult ontogenetic status sex, or taxonomy (see below).

Taxonomic considerations

With the caveats of ontogeny and sex in mind, we found some previously undescribed fossil affinities to KNM-OG 45500. Potts *et al.* (2004) considered KNM-OG 45500 to be most similar to the Dmanisi D2282 near-adult and D2280 adult specimens. In our study, we confirm this similarity in shape (Procrustes distance) to D2282, in addition to affinity to D2700 in size (logCS). We also found that the shape affinities of KNM-OG 45500 to other *H. erectus s.l.* specimens are closer than previously reported in a preceding GM study of the unreconstructed frontal bone (Baab, 2016 Supplement Material). Whereas Baab (2016) found that KNM-OG 45500 was an outlier in shape space in comparison to other Pleistocene *Homo* samples, our results place KNM-OG 45500 within or close to the variation of our sampled *H. erectus s.l.* group. The difference in results with Baab (2016) is likely due, at least in part, to differences in variables used in the analysis, the comparative sample used, and methodological approaches.

Baab (2016) sampled 17 landmarks on the unreconstructed frontal bone, estimating some bilateral landmarks using reflected relabeling (Mardia *et al.*, 2000) of the better-preserved side. However, some landmarks were digitized on the left side, which appears deformed on the lateral posterior margin, while the position of the mid-torus landmark taken on the right side was likely somewhat influenced by the abrasion of the surface. Our reconstruction allowed for greater landmark coverage and accounted for taphonomic distortion of the left side of the frontal squama by using the better preserved right side. However, similar to Baab's results though to a lesser degree, our KNM-OG 45500 reconstructions fell on the margin of *H. erectus s.l.* variability.

Pending more robust attributions of sex and ontogeny for KNM-OG 45500, it is possible that the observed variation in frontal bone form can be linked to taxonomic diversity. Other small-sized *H. erectus s.l.* within Africa are known from the fossil record (Antón, 2004; Rightmire, 2004; Bruner *et al.*, 2015; Semaw *et al.*, 2020). Taxonomic diversity based on differences in cranial size, among other features, has been suggested for early *Homo* groups (Spoor *et al.*, 2015). As a result, Berger *et al.* (2017) have hypothesized that KNM-OG 45500 and OH 12 represent a diverse small-bodied subequatorial hominin lineage culminating in the more recent *H. naledi* specimens in South Africa. Our results support this hypothesis only to the extent that both our cluster analysis and the logCS values highlight similar morphology and size between KNM-OG 45500 and *H. naledi*. Moreover, KNM-OG 45500 and Daka BOU-VP-2/66, which are close in both chronology and geography (Asfaw *et al.*, 2002; Potts *et al.*, 2004; Gilbert & Asfaw, 2008) are different not only in their size, but also in shape when we consider all the reconstructions made with the estimation of bregma. KNM-OG 45500 has a more shelf-like morphology compared to Daka BOU-VP-2/66 and a thin supraorbital torus. Despite this evidence, our overall results do not support a different taxonomic attribution of KNM-OG

45500 from the one proposed by Potts and colleagues (2004). Both in terms of its positioning in shape space and pairwise Procrustes distance, KNM-OG 45500 is more distant from the *H. naledi* specimen than from other *H. erectus s.l.* fossils, especially the early Pleistocene African and Georgian specimens. For this reason, we cannot reject the hypothesis that KNM-OG 45500 belongs to the *H. erectus* hypodigm. Future work in eastern Africa and the inclusion of newly discovered hominin remains excavated at Olororgesale could shed light on local patterns of cranial form evolution and allow further comparison with other Pleistocene *Homo* fossils across Africa.

Patterns of variation in H. erectus s.l.

Another aspect that is important to note is the presence of continuity of frontal bone shape in Africa. This continuum in frontal bone morphology presumably appeared with the emergence of *Homo erectus s.l.* diagnostic features, expressed in specimens like KNM-ER 3733, and lasted up to about 1 Ma, represented in our study by KNM-OG 45500. Beginning in the Middle Pleistocene, some fossils then show a more derived morphology. Our results show this to the extent that Middle to Late Pleistocene fossils across Africa and Eurasia are distinct from the Early Pleistocene fossils along the major axis of variation in shape space (i.e. along PC1 in Fig. 4), consistent with previous GM studies on cranial form (Manzi *et al.*, 2003; Baab, 2015, 2016; Manzi, 2016; Profico *et al.*, 2016). The UPGMA phenogram (Fig. 5) also shows two temporal clusters that split our fossil sample primarily by chronology, from early specimens dated to between ca. 1.77 to 0.7 Ma BP to more derived specimens dated to between the Middle and Late Pleistocene. The Early Pleistocene *Au. sediba* and Middle Pleistocene *H. naledi* specimens seem to contradict the pattern seen in the shape analysis. Whereas the positioning of *Au. sediba* is likely associated in part to its sub-adult stage, the positioning of the *H. naledi* specimen might indeed be indicative of distinct taxonomy or greater anatomical variation in Pleistocene

Homo than previously considered (Berger *et al.*, 2017; Schroeder *et al.*, 2017). However, we caution that our observations might be biased by the composite reconstruction, which includes both the *H. naledi* DH1 holotype & DH3 paratype.

Looking at the *H. erectus s.l.* fossils, our results seem to cluster specimens in different paleodemes (Howell, 1999). In this sense, the African early Pleistocene Nariokotome paleodeme (Howell, 1999) seems to be relatively homogeneous until ca. 1 Ma, comprising also KNM-OG 45500 and Daka BOU-VP-2/66. In Eurasia, the Dmanisi paleodeme is not very different in frontal morphology from the African Nariokotome paleodeme. Asian paleodemes from Sangiran, Zhoukoutien, and Ngandong seem to express a morphological trajectory that is initially similar to the Early Pleistocene African Eurasian morphology (Sangiran 17, associated with a low PC1 score in Fig. 4) and subsequently becomes more derived (Zhoukoutien and Ngandong, associated with higher PC1 values in Fig. 4) later in time. However, caution is required in drawing such conclusions since we are only sampling one or two specimens for each paleodeme. Moreover, no full consensus exists about the relationships among these paleodemes (Openoorth, 1932; Weidenreich, 1951; Stringer, 1984; Wolpoff *et al.*, 1994; Delson *et al.*, 2001; Widiyanto & Zeitoun, 2003; Zeitoun *et al.*, 2010; Schwartz & Tattersall, 2015; Tattersall, 2015; Rightmire *et al.*, 2019). Nevertheless, the high variability expressed by *H. erectus s.l.* is often linked to the great geochronological and associated paleoenvironmental spread of the taxon, spanning from the Early to Late Pleistocene of Africa and Southeast Asia (Antón *et al.* 2014).

The Sambungmacan 3 specimen is of particular interest in the context of our results. Dated from a context possibly as late as 70-40 ka (Yokoyama *et al.*, 2008), it shows a more derived frontal morphology compared to the Ngandong specimen, which comes from a context dated to ca. 118-108 ka (Rizal *et al.*, 2020). Despite their close origin and chronology, Sambungmacan 3 shows closer morphological affinities to the Jebel Irhoud 1 and Skhul V specimens. Consistent

with previous observations (Delson *et al.*, 2001), our results show that Sambungmacan 3 has a relatively rounded frontal squama (i.e. high PC1 scores in Figs. 3,4), distinct from other *H. erectus s.l.* fossils. These results might indicate a taxonomic difference between earlier *H. erectus* and Sambungmacan 3, which might be interpreted as an “evolved lineage” of *H. erectus*. Previous works have found that this specimen, as well as other late Javan individuals from Ngandong, are at the extreme of *H. erectus* variability (Weidenreich, 1951; Delson *et al.*, 2001; Widiyanto & Zeitoun, 2003; Zeitoun *et al.*, 2010; Baab, 2016), so that some authors proposed that they might represent a different taxon, *H. sapiens soloensis* or *H. soloensis* (Openoorth, 1932; Widiyanto & Zeitoun, 2003; Zeitoun *et al.*, 2010). This view is analogous to the debate on taxonomic diversity in eastern Africa *H. erectus s.l.* fossils. Compared to Zeitoun *et al.* (2010), our analysis did not include the full fossil series from Ngandong and Sambungmacan, nor the full available morphology of these specimens. Our results, therefore, might differ from theirs for this reason. Similar to that study, however, we found Sambungmacan 3 to be closer to Jebel Irhoud 1 in our PCA plot and to Skhul V in terms of Procrustes distance. Future analysis should investigate further the relationship between all the fossils from Java in order to better assess morphological variation in that series.

Interestingly, Sambungmacan 3 is also close to the Aboriginal Australian individuals from the comparative modern human sample in our study. Genomic research on recent Southeast Asian and Aboriginal Australian populations have found evidence of genetic introgression from Pleistocene populations, including Denisovans, Neanderthals, and possibly a third hominin group (Malaspinas *et al.*, 2016; Jacobs *et al.*, 2019; Mondal *et al.*, 2019). Moreover, some evidence suggests that Aboriginal Australians may descend from the first modern humans who dispersed into Oceania between 70 and 50 ka (Rasmussen *et al.*, 2011; Reyes-Centeno *et al.*, 2014). In light of this, it is interesting to note that the Australian individuals sampled

in our analysis plot closer to the hominin fossils along PC1 and PC2 (crossed diamond in Fig. 3) compared to the other modern humans sampled. Moreover, Australians are particularly close in Procrustes distances to Sambungmacan 3 and to other fossils. Although these similarities could be due to bias in our sampling strategy, the cranial phenotype is known to be linked to the genotype such that genetic introgression events may influence cranial morphology of modern humans (Reyes-Centeno *et al.*, 2014; Gunz *et al.*, 2019). Therefore, future work should aim to test the hypothesis that Sambungmacan 3 might represent evidence of admixture between hominin groups. The implication is that gene flow is an important factor to consider in the high morphological variation of *H. erectus s.l.*, both in the Early Pleistocene of eastern Africa at one extreme and in the Late Pleistocene of Southeast Asia and Oceania at the other extreme.

Limitations and future research directions

Our analyses are limited by two main factors. The first is that analysis of the frontal bone shape alone might not be sufficient to capture the phylogenetic relationships between different fossil groups (Terhune *et al.*, 2007; Baab, 2016; Schroeder *et al.*, 2017). Future work should therefore also analyze KNM-OG 45500's temporal bone fragment in order to evaluate differences and similarities to other fossils and to further test the conclusions drawn from our analyses. We note that while temporal bone morphology has been suggested to be particularly important in tracing population history in both modern humans (Harvati & Weaver, 2006a; Smith *et al.*, 2007; Reyes-Centeno *et al.*, 2017) and hominins (Lockwood *et al.*, 2004, 2005; Harvati & Weaver, 2006b; Terhune *et al.*, 2007), the frontal bone has been suggested to better reflect phylogenetic relationships across hominoid taxa (von Cramon-Taubadel & Smith, 2012). Second, we were unable to include a number of important specimens in our study, such as the pencontemporaneous Buia UA 31 specimen from Eritrea (Macchiarelli *et al.*, 2004; Bruner *et al.*, 2016) or the later OH 12 specimen from Kenya

(Leakey, 1971). In addition, we were unable to include the small-sized specimens from eastern Africa (e.g. DAN5/P1 and KNM-ER 42700) or from Southeast Asia (e.g. Ngandong and Liang Bua 1 (Brown *et al.*, 2004)), variably assigned to *H. erectus s.l.* or to distinct taxa. The frontal bones of all of these specimens either require further reconstruction for appropriate comparison or they were not available for this study. Future work should therefore focus on a broader comparison, aiming for the comprehensive analysis of incomplete specimens.

Conclusions

In summary, our results show that the KNM-OG 45500 frontal bone exhibits affinities to Early Pleistocene fossils from both Africa and Eurasia in its form. In both its shape and size, it is most similar to Early Pleistocene specimens taxonomically assigned to *H. erectus/ergaster*. Overall, our results concur with the original attribution of KNM-OG 45500 to *H. erectus s.l.* and similarly highlight how KNM-OG 45500 extends the taxon's range of size variation for this time period. Based on its small size, KNM-OG 45500 might be considered female, although the relationship of size, shape, and sexual dimorphism in *H. erectus s.l.* must be explored further. Finally, the possibility that this specimen is part of a lineage culminating in the South African *H. naledi* remains open. It is therefore important to consider KNM-OG 45500 in future research on the evolution of Pleistocene *Homo*, and the reconstruction introduced here will allow its inclusion in future studies. We expect that additional work with the KNM-OG 45500 temporal bone, including more comprehensive cranial reconstruction efforts, will further shed light on the diversity of Pleistocene hominins and clarify the *H. erectus* hypodigm.

Data sharing

The raw dataset and R code used can be provided by the corresponding author upon request.

3D surfaces used cannot be provided due to copyright restriction and license agreement with institutions.

Acknowledgments

We thank the following institutions and colleagues for access to fossil comparative material: Richard Potts and colleagues at the Smithsonian Institution, as well as Fredrick Mantshi, Timothy Gichunge, and the members of the Department of Earth Science, National Museums of Kenya for access to the KNM-OG 45500 surface scan and CT scans of KNM-ER 3733 and KNM-ER 3883; Gen Suwa, the Authority for Research and Conservation of Cultural Heritage (ARCCCH), and the National Museum of Ethiopia for providing the Daka calvarium (BOU-VP-2/66) external mesh reconstruction; Sabine Eggers for access to CT scan from the Department of Anthropology of the Naturhistorisches Museum in Vienna; Giselle Garcia and Eric Delson, American Museum of Natural History; Monica Zavattaro and Jacopo Moggi-Cecchi for access to the CT scans from the Anthropological Collection at the Museo di Storia Naturale dell'Università di Firenze; Antoine Balzeau, Martin Friess, and Dominique Grimaud-Hervé for access to the CT scans from the Muséum national d'Histoire naturelle, Paris. The *Skhül V* fossil scan was downloaded from the Peabody Museum, Harvard University, while the *H. naledi* (DH1 & DH3) and *A. sediba* (MH1) scans were downloaded from the MorphoSource database, Duke University (media number: M7300-8170). We thank Marlijn Noback for providing access to scans of the modern human comparative sample, as well as Yonatan Sable for facilitating access to the Daka CT scan and for helpful discussion on this project. Finally, we thank Hannes Rathmann for his help in the figures' production. This work was funded in part by the German Research Foundation (DFG-INST-371706-1 FUGG and DFG-FOR-2237: "Words, Bones, Genes, Tools: Tracking Linguistic, Cultural, and Biological Trajectories of the Human Past").

Author contributions

KH and TM conceptualized and designed the study. TM collected the data. TM and AP analyzed the data. TM, AP, HRC, KH interpreted and commented on the results of the analyses. TM drafted the manuscript. HRC, KH, AP revised and edited extensively the whole manuscript. All authors read, provided feedback and approved the manuscript.

References

- Antón S.C. 2003. Natural history of *Homo erectus*. *Am. J. Phys. Anthropol.*, 122: 126-170.
- Antón S.C. 2004. The face of Olduvai hominid 12. *J. Hum. Evol.*, 46: 335-345.
- Antón S.C. 2007. Defining *Homo erectus*: size considered. *Handbook of Paleoanthropology*, 3: Chapter 11.
- Antón S.C., Potts R. & Aiello L.C. 2014. Evolution of early *Homo*: An integrated biological perspective. *Science*, 345: 1236828.
- Arsuaga J.L., Carretero J.M., Lorenzo C. *et al.* 1997. Size Variation in Middle Pleistocene Humans. *Science*, 277: 1086-1088.
- Asfaw B., Gilbert W.H., Beyene Y. *et al.* 2002. Remains of *Homo erectus* from Bouri, Middle Awash, Ethiopia. *Nature*, 416: 317.
- Athreya S. 2012. The frontal bone in the genus *Homo*: a survey of functional and phylogenetic sources of variation. *J. Anthropol. Sci.*, 90: 1-22.
- Aytek A.İ. & Harvati K. 2016. The human fossil record from Turkey. In K. Harvati & M. Roksandic (eds): *Paleoanthropology of the Balkans and Anatolia*, pp. 79-91. Springer, Dordrecht.
- Baab K.L. 2008a. A re-evaluation of the taxonomic affinities of the early *Homo* cranium KNM-ER 42700. *J. Hum. Evol.*, 55: 741-746.
- Baab K.L. 2008b. The taxonomic implications of cranial shape variation in *Homo erectus*. *J. Hum. Evol.*, 54: 827-847.
- Baab K.L. 2015. Defining *Homo erectus*. In W. Henke & I. Tattersall (eds): *Handbook of*

- paleoanthropology*, pp. 2189-2219. Springer, Berlin, Heidelberg.
- Baab K.L. 2016. The role of neurocranial shape in defining the boundaries of an expanded *Homo erectus* hypodigm. *J. Hum. Evol.*, 92: 1-21.
- Bauer C.C. & Harvati K. 2015. A virtual reconstruction and comparative analysis of the KNM-ER 42700 cranium. *Anthrop. Anz.*, 72: 129-140.
- Berger L.R., de Ruiter D.J., Churchill S.E. et al. 2010. *Australopithecus sediba*: A New Species of *Homo*-Like Australopith from South Africa. *Science*, 328: 195-204.
- Berger L.R., Hawks J., de Ruiter D.J. et al. 2015. *Homo naledi*, a new species of the genus *Homo* from the Dinaledi Chamber, South Africa. *Elife*, 4: e09560.
- Berger L.R., Hawks J., Dirks P.H. et al. 2017. *Homo naledi* and Pleistocene hominin evolution in subequatorial Africa. *Elife*, 6: e24234.
- Bookstein F.L. 1989. Principal warps: Thin-plate splines and the decomposition of deformations. *IEEE Transactions on pattern analysis and machine intelligence*, 11: 567-585.
- Bookstein F.L. 1991. *Morphometric tools for landmark data: geometry and biology*. Cambridge University Press, Cambridge.
- Bosman A., Buck L., Reyes-Centeno H. et al. 2019. The Kabua I cranium: Virtual anatomical reconstructions In Y. Sahle, H. Reyes-Centeno & C. Bentz (eds): *Modern Human Origins and Dispersal*. Kerns Verlag, Tuebingen.
- Bosman A.M., Reyes-Centeno H. & Harvati K. 2020. A virtual assessment of the suprainiac depressions on the Eyasi I (Tanzania) and Aduma ADU-VP-1/3 (Ethiopia) Pleistocene hominin crania. *J. Hum. Evol.*, 145: 102815.
- Brown P., Sutikna T., Morwood M.J. et al. 2004. A new small-bodied hominin from the Late Pleistocene of Flores, Indonesia. *Nature*, 431: 1055.
- Bruner E., Bondioli L., Coppa A. et al. 2016. The endocast of the one-million-year-old human cranium from Buia (UA 31), Danakil Eritrea. *Am. J. Phys. Anthropol.*, 160: 458-468.
- Bruner E., Grimaud-Hervé D., Wu X. et al. 2015. A paleoneurological survey of *Homo erectus* endocranial metrics. *Quat. Int.*, 368: 80-87.
- Buck L.T. & Stringer C.B. 2015. A rich locality in South Kensington: the fossil hominin collection of the Natural History Museum, London. *Geological Journal*, 50: 321-337.
- Cignoni P., Callieri M., Corsini M. et al. 2008. Meshlab: an open-source mesh processing tool. In: *Eurographics Italian chapter conference*, p. 129-136.
- Delson E., Harvati K., Reddy D. et al. 2001. The Sambungmacan 3 *Homo erectus* calvaria: a comparative morphometric and morphological analysis. *Anat. Rec. (Hoboken)*, 262: 380-397.
- Détroit F., Mijares A.S., Corny J. et al. 2019. A new species of *Homo* from the Late Pleistocene of the Philippines. *Nature*, 568: 181.
- Dirks P.H., Roberts E.M., Hilbert-Wolf H. et al. 2017. The age of *Homo naledi* and associated sediments in the Rising Star Cave, South Africa. *Elife*, 6: e24231.
- Dubois M.E.F.T. 1894. *Pithecanthropus erectus: eine menschenähnliche Übergangsform aus Java*. Landesdruckerei.
- Freidline S.E., Gunz P., Janković I. et al. 2012. A comprehensive morphometric analysis of the frontal and zygomatic bone of the Zuttiyeh fossil from Israel. *J. Hum. Evol.*, 62: 225-241.
- Garcia T., Féraud G., Falguères C. et al. 2010. Earliest human remains in Eurasia: New 40Ar/39Ar dating of the Dmanisi hominid-bearing levels, Georgia. *Quat. Geochronol.*, 5: 443-451.
- Gibbard P.L., Head M.J., Walker M.J. et al. 2010. Formal ratification of the Quaternary System/Period and the Pleistocene Series/Epoch with a base at 2.58 Ma. *J. Quat. Sci.*, 25: 96-102.
- Gilbert W.H. & Asfaw B. 2008. *Homo erectus: Pleistocene Evidence from the Middle Awash, Ethiopia*. University of California Press, Berkeley and Los Angeles, California.
- Gower J.C. 1975. Generalized procrustes analysis. *Psychometrika*, 40: 33-51.
- Grabowski M., Hatala K.G., Jungers W.L. et al. 2015. Body mass estimates of hominin fossils

- and the evolution of human body size. *J. Hum. Evol.*, 85: 75-93.
- Grün R. 1996. A re-analysis of electron spin resonance dating results associated with the Petralona hominid. *J. Hum. Evol.*, 30: 227-241.
- Grün R. 2006. Direct dating of human fossils. *Am. J. Phys. Anthropol.*, 131: 2-48.
- Grün R. & Stringer C.B. 1991. Electron spin resonance dating and the evolution of modern humans. *Archaeometry*, 33: 153-199.
- Gunz P., Mitteroecker P. & Bookstein F.L. 2005. Semilandmarks in three dimensions. In D.E. Slice (ed): *Modern morphometrics in physical anthropology*, pp. 73-98. Springer, Boston, MA.
- Gunz P., Mitteroecker P., Neubauer S. *et al.* 2009. Principles for the virtual reconstruction of hominin crania. *J. Hum. Evol.*, 57: 48-62.
- Gunz P., Neubauer S., Maureille B. *et al.* 2010. Brain development after birth differs between Neanderthals and modern humans. *Curr. Biol.*, 20: R921-R922.
- Gunz P., Tilot A.K., Wittfeld K. *et al.* 2019. Neandertal introgression sheds light on modern human endocranial globularity. *Curr. Biol.*, 29: 120-127. e125.
- Harvati K., Röding C., Bosman A.M. *et al.* 2019. Apidima Cave fossils provide earliest evidence of *Homo sapiens* in Eurasia. *Nature*, 571: 500-504.
- Harvati K. & Weaver T.D. 2006a. Human cranial anatomy and the differential preservation of population history and climate signatures. *Anat. Rec. (Hoboken)*, 288A: 1225-1233.
- Harvati K. & Weaver T.D. 2006b. Reliability of cranial morphology in reconstructing Neanderthal phylogeny. In J.J. Hublin, K. Harvati & T. Harrison (eds): *Neanderthals revisited: new approaches and perspectives*, pp. 239-254. Springer, Dordrecht.
- Howell F.C. 1999. Paleo-Demes, Species Clades, and Extinctions in the Pleistocene Hominin Record. *J. Anthropol. Res.*, 55: 191-243.
- Jacobs G.S., Hudjashov G., Saag L. *et al.* 2019. Multiple Deeply Divergent Denisovan Ancestries in Papuans. *Cell*, 177: 1010-1021. e1032.
- Kidder J.H. & Durband A.C. 2004. A re-evaluation of the metric diversity within *Homo erectus*. *J. Hum. Evol.*, 46: 297-313.
- Larick R., Ciochon R.L., Zaim Y. *et al.* 2001. Early Pleistocene 40Ar/39Ar ages for Bapang formation hominins, central Jawa, Indonesia. *Proc. Natl. Acad. Sci. USA*, 98: 4866-4871.
- Leakey M.D. 1971. *Olduvai Gorge: Volume 3, excavations in beds I and II, 1960-1963*. Cambridge University Press, Cambridge.
- Leakey M.G., Spoor F., Dean M.C. *et al.* 2012. New fossils from Koobi Fora in northern Kenya confirm taxonomic diversity in early *Homo*. *Nature*, 488: 201.
- Lepre C.J. & Kent D.V. 2015. Chronostratigraphy of KNM-ER 3733 and other Area 104 hominins from Koobi Fora. *J. Hum. Evol.*, 86: 99-111.
- Lieberman D.E. 2011. *The evolution of the human head*. The belknap press of Harvard University Press.
- Lockwood C.A., Kimbel W.H. & Lynch J.M. 2004. Morphometrics and hominoid phylogeny: Support for a chimpanzee-human clade and differentiation among great ape subspecies. *Proc. Natl. Acad. Sci. USA*, 101: 4356-4360.
- Lockwood C.A., Kimbel W.H. & Lynch J.M. 2005. Variation in early hominin temporal bone morphology and its implications for species diversity. *Trans. R. Soc. S. Afr.*, 60: 73-77.
- Lordkipanidze D., Ponce de León M.S., Margvelashvili A. *et al.* 2013. A Complete Skull from Dmanisi, Georgia, and the Evolutionary Biology of Early *Homo*. *Science*, 342: 326-331.
- Macchiarelli R., Bondioli L., Chech M. *et al.* 2004. The late early Pleistocene human remains from Buia, Danakil depression, Eritrea. *Rivista Italiana di Paleontologia e Stratigrafia (Research In Paleontology and Stratigraphy)*, 110.
- Malaspina A.-S., Westaway M.C., Muller C. *et al.* 2016. A genomic history of Aboriginal Australia. *Nature*, 538: 207-214.
- Manzi G. 2016. Humans of the Middle Pleistocene: The controversial calvarium from

- Ceprano (Italy) and its significance for the origin and variability of *Homo heidelbergensis*. *Quat. Int.*, 411: 254-261.
- Manzi G., Bruner E. & Passarelli P. 2003. The one-million-year-old *Homo* cranium from Bouri (Ethiopia): a reconsideration of its *H. erectus* affinities. *J. Hum. Evol.*, 44: 731-736.
- Mardia K.V., Bookstein F.L. & Moreton I.J. 2000. Statistical assessment of bilateral symmetry of shapes. *Biometrika*, 87: 285-300.
- Matsu'ura S., Kondo M., Danhara T. et al. 2020. Age control of the first appearance datum for Javanese *Homo erectus* in the Sangiran area. *Science*, 367: 210-214.
- McDougall I., Brown F.H., Vasconcelos P.M. et al. 2012. New single crystal ⁴⁰Ar/³⁹Ar ages improve time scale for deposition of the Omo Group, Omo-Turkana Basin, East Africa. *J. Geol. Soc. London*, 169: 213-226.
- Meindl R.S. & Lovejoy C.O. 1985. Ectocranial suture closure: a revised method for the determination of skeletal age at death based on the lateral-anterior sutures. *Am. J. Phys. Anthropol.*, 68: 57-66.
- Mitteroecker P. & Bookstein F. 2011. Linear discrimination, ordination, and the visualization of selection gradients in modern morphometrics. *Evol. Biol.*, 38: 100-114.
- Mitteroecker P. & Gunz P. 2009. Advances in Geometric Morphometrics. *Evol. Biol.*, 36: 235-247.
- Mondal M., Bertranpetit J. & Lao O. 2019. Approximate Bayesian computation with deep learning supports a third archaic introgression in Asia and Oceania. *Nat. Comm.*, 10: 1-9.
- Mori T. & Harvati K. 2019. Basicranial ontogeny comparison in *Pan troglodytes* and *Homo sapiens* and its use for developmental stage definition of KNM-ER 42700. *Am. J. Phys. Anthropol.*, 170: 579-594
- Neeser R., Ackermann R.R. & Gain J. 2009. Comparing the accuracy and precision of three techniques used for estimating missing landmarks when reconstructing fossil hominin crania. *Am. J. Phys. Anthropol.*, 140: 1-18.
- Neubauer S., Gunz P. & Hublin J.-J. 2010. Endocranial shape changes during growth in chimpanzees and humans: A morphometric analysis of unique and shared aspects. *J. Hum. Evol.*, 59: 555-566.
- Neubauer S., Gunz P., Leakey L. et al. 2018. Reconstruction, endocranial form and taxonomic affinity of the early *Homo* calvaria KNM-ER 42700. *J. Hum. Evol.*, 121: 25-39.
- Noback M.L. & Harvati K. 2014. Covariation in the Human Masticatory Apparatus. *Anat. Rec. (Hoboken)*, 298: 64-84.
- Noback M.L. & Harvati K. 2015. The contribution of subsistence to global human cranial variation. *J. Hum. Evol.*, 80: 34-50.
- Openoorth W. 1932. *Homo (Javanthropus) soloensis*, een pleistoocene mensch van Java. *Wetesch Mededee. Dienst Mijnbouw Nederl Indie*, 20: 49-74.
- Pickering R., Dirks P.H., Jinnah Z. et al. 2011. *Australopithecus sediba* at 1.977 Ma and implications for the origins of the genus *Homo*. *Science*, 333: 1421-1423.
- Plavcan J.M. 2012. Body size, size variation, and sexual size dimorphism in early *Homo*. *Curr. Anthropol.*, 53: S409-S423.
- Ponce De Leon M.S. & Zollikofer C.P. 1999. New evidence from Le Moustier I: Computer-assisted reconstruction and morphometry of the skull. *Anat. Rec. (Hoboken)*, 254: 474-489.
- Potts R., Behrensmeier A.K., Deino A. et al. 2004. Small Mid-Pleistocene Hominin Associated with East African Acheulean Technology. *Science*, 305: 75-78.
- Profico A., Di Vincenzo F., Gagliardi L. et al. 2016. Filling the gap. Human cranial remains from Gombore II (Melka Kunture, Ethiopia; ca. 850 ka) and the origin of *Homo heidelbergensis*. *J. Anthropol. Sci.*, 94: 1-24.
- Profico A., Schlager S., Valoriani V. et al. 2018. Reproducing the internal and external anatomy of fossil bones: Two new automatic digital tools. *Am. J. Phys. Anthropol.*, 166: 979-986.
- R Core Team. 2018. *R: A language and environment for statistical computing*.
- Rasmussen M., Guo X., Wang Y. et al. 2011. An Aboriginal Australian genome reveals separate human dispersals into Asia. *Science*, 334: 94-98.

- Reyes-Centeno H., Ghirotto S., Détroit F. *et al.* 2014. Genomic and cranial phenotype data support multiple modern human dispersals from Africa and a southern route into Asia. *Proc. Natl. Acad. Sci. USA*, 111: 7248-7253.
- Reyes-Centeno H., Ghirotto S. & Harvati K. 2017. Genomic validation of the differential preservation of population history in modern human cranial anatomy. *Am. J. Phys. Anthropol.*, 162: 170-179.
- Richter D., Grün R., Joannes-Boyau R. *et al.* 2017. The age of the hominin fossils from Jebel Irhoud, Morocco, and the origins of the Middle Stone Age. *Nature*, 546: 293.
- Rightmire G.P. 1979. Cranial remains of *Homo erectus* from Beds II and IV, Olduvai Gorge, Tanzania. *Am. J. Phys. Anthropol.*, 51: 99-115.
- Rightmire G.P. 1981. Patterns in the evolution of *Homo erectus*. *Paleobiology*, 7: 241-246.
- Rightmire G.P. 1990. *The Evolution of Homo Erectus: Comparative Anatomical Studies of an Extinct Human Species*. Cambridge University Press, Cambridge.
- Rightmire G.P. 2004. Brain size and encephalization in early to mid-Pleistocene *Homo*. *Am. J. Phys. Anthropol.*, 124: 109-123.
- Rightmire G.P. 2013. *Homo erectus* and Middle Pleistocene hominins: brain size, skull form, and species recognition. *J. Hum. Evol.*, 65: 223-252.
- Rightmire G.P., Lordkipanidze D. & Vekua A. 2006. Anatomical descriptions, comparative studies and evolutionary significance of the hominin skulls from Dmanisi, Republic of Georgia. *J. Hum. Evol.*, 50: 115-141.
- Rightmire G.P., Margvelashvili A. & Lordkipanidze D. 2019. Variation among the Dmanisi hominins: Multiple taxa or one species? *Am. J. Phys. Anthropol.*, 168: 481-495.
- Rightmire P.G. 1996. The human cranium from Bodo, Ethiopia: evidence for speciation in the Middle Pleistocene? *J. Hum. Evol.*, 31: 21-39.
- Rizal Y., Westaway K.E., Zaim Y. *et al.* 2020. Last appearance of *Homo erectus* at Ngandong, Java, 117,000–108,000 years ago. *Nature*, 577: 381-385.
- Rohlf F.J. & Slice D. 1990. Extensions of the Procrustes Method for the Optimal Superimposition of Landmarks. *Syst. Biol.*, 39: 40-59.
- Schlager S. 2017. Morpho and Rvcg–Shape Analysis in R: R-Packages for geometric morphometrics, shape analysis and surface manipulations. In G. Zheng, S. Li & G. Székely (eds): *Statistical shape and deformation analysis*, pp. 217-256. Academic Press, Cambridge.
- Schliep K.P. 2010. phangorn: phylogenetic analysis in R. *Bioinformatics*, 27: 592-593.
- Schroeder L., Scott J.E., Garvin H.M. *et al.* 2017. Skull diversity in the *Homo* lineage and the relative position of *Homo naledi*. *J. Hum. Evol.*, 104: 124-135.
- Schwartz J.H. 2004. Getting to Know *Homo erectus*. *Science*, 305: 53.
- Schwartz J.H. & Tattersall I. 2000. What constitutes *Homo erectus*. *Acta Anthropol. Sin.*, 19: 18-22.
- Schwartz J.H. & Tattersall I. 2015. Defining the genus *Homo*. *Science*, 349: 931-932.
- Scott N., Neubauer S., Hublin J.-J. *et al.* 2014. A Shared Pattern of Postnatal Endocranial Development in Extant Hominoids. *Evol. Biol.*, 41: 572-594.
- Semaw S., Rogers M.J., Simpson S.W. *et al.* 2020. Co-occurrence of Acheulian and Oldowan artifacts with *Homo erectus* cranial fossils from Gona, Afar, Ethiopia. *Sci. Adv.*, 6: eaaw4694.
- Shen G., Gao X., Gao B. *et al.* 2009. Age of Zhoukoudian *Homo erectus* determined with ²⁶Al/¹⁰Be burial dating. *Nature*, 458: 198-200.
- Slice D.E. 2007. Geometric Morphometrics. *Annu. Rev. Anthropol.*, 36: 261-281.
- Smith H.F. 2009. Which cranial regions reflect molecular distances reliably in humans? Evidence from three-dimensional morphology. *Am. J. Hum. Biol.*, 21: 36-47.
- Smith H.F., Terhune C.E. & Lockwood C.A. 2007. Genetic, geographic, and environmental correlates of human temporal bone variation. *Am. J. Phys. Anthropol.*, 134: 312-322.
- Sokal R.R. 1958. A statistical method for evaluating systematic relationships. *Univ. Kansas, Sci. Bull.*, 38: 1409-1438.

- Spoor F., Gunz P., Neubauer S. et al. 2015. Reconstructed *Homo habilis* type OH 7 suggests deep-rooted species diversity in early Homo. *Nature*, 519: 83.
- Spoor F., Leakey M.G., Gathogo P.N. et al. 2007. Implications of new early Homo fossils from Ileret, east of Lake Turkana, Kenya. *Nature*, 448: 688.
- Stringer C.B. 1984. The definition of *Homo erectus* and the existence of the species in Africa and Europe. *Cour. Forsch. Inst. Senckenberg, Frankfurt am Main*, 69: 131-143.
- Suwa G.E.N., Asfaw B., Haile-Selassie Y. et al. 2007. Early Pleistocene *Homo erectus* fossils from Konso, southern Ethiopia. *Anthropol. Sci.*, 115: 133-151.
- Tamrat E., Thouveny N., Tai M. et al. 1995. Revised magnetostratigraphy of the Plio-Pleistocene sedimentary sequence of the Olduvai Formation (Tanzania). *Palaeogeogr., Palaeoclimatol., Palaeoecol.*, 114: 273-283.
- Tattersall I. 1992. Species concepts and species identification in human evolution. *J. Hum. Evol.*, 22: 341-349.
- Tattersall I. 2015. *Homo ergaster* and Its Contemporaries. In W. Henke & I. Tattersall (eds): *Handbook of Paleoanthropology*, pp. 2167-2187. Springer Berlin Heidelberg.
- Terhune C.E., Kimbel W.H. & Lockwood C.A. 2007. Variation and diversity in *Homo erectus*: a 3D geometric morphometric analysis of the temporal bone. *J. Hum. Evol.*, 53: 41-60.
- Terhune C.E., Kimbel W.H. & Lockwood C.A. 2013. Postnatal temporal bone ontogeny in Pan, Gorilla, and Homo, and the implications for temporal bone ontogeny in *Australopithecus afarensis*. *Am. J. Phys. Anthropol.*, 151: 630-642.
- Vekua A., Lordkipanidze D., Rightmire G.P. et al. 2002. A New Skull of Early Homo from Dmanisi, Georgia. *Science*, 297: 85-89.
- Villmoare B., Hatala K.G. & Jungers W. 2019. Sexual dimorphism in *Homo erectus* inferred from 1.5 Ma footprints near Ileret, Kenya. *Sci. Rep.*, 9: 7687.
- von Cramon-Taubadel N. 2009. Congruence of individual cranial bone morphology and neutral molecular affinity patterns in modern humans. *Am. J. Phys. Anthropol.*, 140: 205-215.
- von Cramon-Taubadel N. & Smith H.F. 2012. The relative congruence of cranial and genetic estimates of hominoid taxon relationships: Implications for the reconstruction of hominin phylogeny. *J. Hum. Evol.*, 62: 640-653.
- Weber G.W. 2015. Virtual anthropology. *Am. J. Phys. Anthropol.*, 156: 22-42.
- Weber G.W. & Bookstein F.L. 2011. *Virtual anthropology: a guide to a new interdisciplinary field*. Springer, New York, Wien.
- Weidenreich F. 1940. *The torus occipitalis and related structures and their transformations in the course of human evolution*. Geological Soc. of China.
- Weidenreich F. 1951. Morphology of Solo man. *Anthropological Paper of the American Museum of Natural History*, 43: 205-290.
- Widianto H. & Zeitoun V. 2003. Morphological description, biometry and phylogenetic position of the skull of Ngawi 1 (east Java, Indonesia). *Int. J. Osteoarch.*, 13: 339-351.
- Wolpoff M.H., Thorne A.G., Jelinek J. et al. 1994. The case for sinking *Homo erectus*: 100 years of *Pithecanthropus* is enough. *Cour. Forschungsinst. Senckenb.*, 171: 341-361.
- Wood B. 1991. *Koobi Fora research project: Hominid cranial remains*. Oxford University Press, USA.
- Wood B. 1992. Origin and evolution of the genus *Homo*. *Nature*, 355: 783.
- Wood B. 1994. Taxonomy and evolutionary relationships of *Homo erectus*. *Cour. Forschungsinst. Senckenb.*, 171: 159-165.
- Wood B. & Richmond B.G. 2000. Human evolution: taxonomy and paleobiology. *J. Anat.*, 197: 19-60.
- Wood B.A. 1984. The origin of *Homo erectus*. *Cour. Forsch. Inst. Senckenberg*, 69: 99-111.
- Xiao J., Jin C. & Zhu Y. 2002. Age of the fossil Dali Man in north-central China deduced from chronostratigraphy of the loess-paleosol sequence. *Quat. Sci. Rev.*, 21: 2191-2198.
- Yokoyama Y., Falguères C., Sémah F. et al. 2008. Gamma-ray spectrometric dating of

late *Homo erectus* skulls from Ngandong and Sambungmacan, Central Java, Indonesia. *J. Hum. Evol.*, 55: 274-277.

Zeitoun V., Déroit F, Grimaud-Hervé D. *et al.* 2010. Solo man in question: Convergent

views to split Indonesian *Homo erectus* in two categories. *Quat. Int.*, 223-224: 281-292.

Editor, Giovanni Destro Bisol



This work is distributed under the terms of a Creative Commons Attribution-NonCommercial 4.0 Unported License <http://creativecommons.org/licenses/by-nc/4.0/>